Science of the Total Environment 881 (2023) 163363

Contents lists available at ScienceDirect

Science of the Total Environment

journal homepage: www.elsevier.com/locate/scitotenv

Evaluating the impacts of biochemical processes on nitrogen dynamics in a tide gate-controlled river flowing into the South China Sea

Yinbin Huang [a,b], Zhongya Fan [b,*], Changjin Zhao [b], Gang Chen [b], Ju Huang [b], Zhongbo Zhou [c], Yeyuan Xiao [a,*]

[a] Department of Civil and Environmental Engineering, College of Engineering, Shantou University, Shantou, Guangdong 515063, China
[b] National Key Laboratory of Water Environmental Simulation and Pollution Control, South China Institute of Environmental Sciences, Ministry of Ecology and Environment, Guangzhou 510530, China
[c] College of Resources and Environment, Southwest University, Chongqing 400715, China

HIGHLIGHTS

- NH_4^+-N was chemostatic with respect to discharge in the upstream section.
- NO_3^--N increased while NH_4^+-N decreased with time along the river in dry season.
- The specific substrate concentration decided the rate of the N transformation.
- Along the river, advantage of denitrification over nitrification was enhanced.
- Closed-tide gate improved riverine N removal through nitrification-denitrification.

GRAPHICAL ABSTRACT

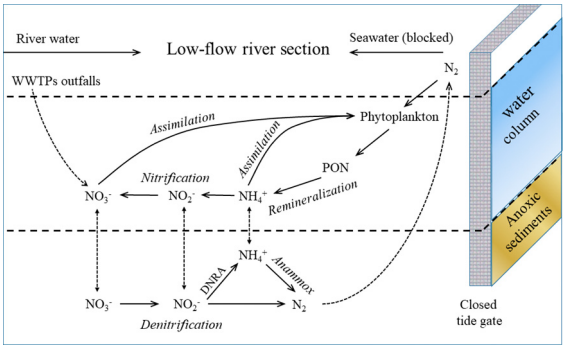

ARTICLE INFO

Editor: Ouyang Wei

Keywords:
Assimilatory nitrate uptake
Nitrogen cycling
Chlorophyll-a
Nitrification-denitrification
Tide gate control
Lianjiang River

ABSTRACT

This study aimed to evaluate the nitrogen (N) dynamics in Lijiang River, a tide gate-controlled river flowing into South China Sea, and to quantify the biochemical processes affecting nitrate fate and transport during the closed-tide gate period. The continuous on-line water monitoring indicates a chemostatic NH_4^+-N pattern with respect to variable discharges in the upstream section. The survey via daily grab water sampling from July to December 2020 at four equidistant locations in the lower stretch showed that a gradual increase in NO_3^--N and decrease in NH_4^+-N concentrations occurred along the river from upstream to downstream sections and with the time from September to December (the closed-tide gate period). The mean difference between nitrification and denitrification rate peaked at 0.43 mg L^{-1} d^{-1} in October in the upper section and gradually reduced to -0.26 mg L^{-1} d^{-1} in December in the middle section, indicating the increased advantage of denitrification over nitrification with time. A gradual increase in the mean NO_3^--N assimilatory uptake rate with time and a decrease from upstream to downstream were also observed. These results show that the closed-tide gate promoted N biotransformation in Laingian River and significant N removal was achieved through coupled nitrification-denitrification.

1. Introduction

Rapid urbanization has greatly altered rivers via impoundments and diversions, and over a half of large river networks is under dams/sluices control (Nilsson et al., 2005; van Looy et al., 2014; Wang et al., 2018). The impacts of dams/sluices construction or demolishment on downstream water conflicts and ecosystem safety have been extensively studied and widely acknowledged. For example, Okyereh et al. (2019) investigated the potential impacts of the development and operation of the Bui Hydropower Dam on downstream water usage competition (domestic, livestock and industrial purposes). Koutrakis et al. (2019) evaluated ecological

* Corresponding authors.
E-mail addresses: fanzhongya@scies.org (Z. Fan), yeyuanxiao@stu.edu.cn (Y. Xiao).

http://dx.doi.org/10.1016/j.scitotenv.2023.163363
Received 21 September 2022; Received in revised form 24 March 2023; Accepted 3 April 2023
Available online 11 April 2023

flows and habitat availability for fishes in the downstream section of dams/sluices in highly regulated Mediterranean rivers. Among the multiple objectives and interests of dams/sluices regulation, flood control and water resource allocation are the top priority. Consequently, dams/sluices operations vary between cycles of dry and wet seasons, thus influencing waste stream discharge, water quality and aquatic ecosystem in the upstream and downstream sections of dams/sluices (Luo et al., 2021).

Tide gates, a kind of dams/sluices installed between estuaries and rivers, are generally doors or flaps mounted on the downstream ends of rivers near the sea, which allow upstream waters to drain while preventing inflows from the sea due to tidal surges or flood events. Different from dams/sluices installed in an inland area, a tide gate experiences rise and fall of water levels in bidirectional flow; water moves toward the land and away from the sea in the flood phase, whereas water flows into the sea during the ebb phase. In flood season, opening tide gates at low tide is launched more often and continues for a longer time; in the dry season, to guarantee the demand of water usage, the tide gates stay closed for most of the time. Therefore, the operation of tide gates has to take account of complicated hydrodynamic conditions and leads to various ecological and environmental consequences (Wright et al., 2015; Zhao et al., 2020). We name the above-mentioned dry season condition as the closed-tide gate period in this study.

When tide gates are closed, contaminants mainly comprised of nitrogen (N) species are released from agricultural lands and wastewater treatment plants (WWTPs) and accumulate in the blocked river sections, thus creating eutrophication, harmful algal blooms, hypoxia, and other ecological problems (Lin et al., 2020; Yu et al., 2020). In contrast, the close of tide gates also prolongs the residence time, enhances particle settling and nutrient transformation and uptake, thus leading to higher N removal (Lembi, 2001). As tide gates are designed and operated for flow regulation, irrespective of accumulation or removal of N pollutants, discharge flows with unpredictable N loads are often generated, threatening the estuary ecosystems (Caraco and Cole, 1999). Considering the increasing demand for dams/sluices globally (Zarfl et al., 2015), there is an urgent need to investigate into the relationship between N pollution and tide gate regulation to propose the best management strategies for environmental sustainability.

When flow conditions are limited by a closed-tide gate, its upstream section serves as a reaction tank, and biochemical processes including assimilatory N uptake, nitrification and denitrification most likely govern N fate. Among the biochemical processes, denitrification is considered the primary pathway for permanent N removal via N_2 gas production (Zhao et al., 2015). Many batch incubation experiments with the addition of inhibitors or isotopes to water column samples has been conducted to determine the rates of individual biochemical processes (Andersson et al., 2006; Damashek et al., 2016; Sebilo et al., 2006). However, these water column studies ignored the interaction of benthic sediments, which have strong influence on nitrification and denitrification (Lehmann et al., 2003; Sebilo et al., 2003; Xia et al., 2008). Moreover, limited samples may not accurately represent the diverse field environments, especially for tide gate-controlled rivers with large spatiotemporal variations on N distribution. To assess the extent of biogeochemical processes in a large-scale river, in situ examination is still considered irreplaceable, despite its difficulties (Kraus et al., 2017).

Therefore, this study investigated the transformation of N species in a tide gate-regulated river during the closed-tide gate period via long-term water grab sampling and on-line water quality monitoring. Since nitrate is both the substrate of denitrification and the product of nitrification and is the sole assimilable N source for most algae and plants (Meyer and Stitt, 2001), nitrate dynamics is crucial in exploring the biochemical processes in riverine N cycle (Jarvie et al., 2018; Kraus et al., 2017). The specific objectives include: 1) to assess the seasonality of N dynamics and impacts of storm events on water quality during the survey year; 2) to quantify the extent of change in nitrate through biochemical processes during the closed-tide gate period; and 3) to unveil the impacts of the tide gate on the upstream N transport and transformation, and to identify key factors controlling assimilatory nitrate uptake, and the coupled nitrification-denitrification. To the best knowledge of the authors, this study is the first-of-its-kind to conduct in-situ investigation into N transformation in tide gate-regulated rivers and shall shed new light on sustainable management of estuaries.

2. Materials and methods

2.1. Site description

The Lianjiang River is major river in eastern Guangdong, China, flowing through the two cities of Jieyang and Shantou. It has a catchment area of 1353 km^2, and the center of the basin is located at 116.33°E, 23.26°N. The mainstream is 71 km in length, connecting inland Puning City at 166.15°E, 23.36°N and the South China Sea at the HaiMen Bay (HMB), where the tide gate is located 2 km away from the river mouth (Fig. 1). The annual average runoff of the river is 1.353 billion m^3 and the average annual rainfall is 1618 mm. The rainfall was unevenly distributed throughout the year, with a lower amount in winter and spring (~36.1 % of precipitation) and a higher amount in summer and autumn (~63.9 % of precipitation). The strong seasonal variation in rainfall is related to the subtropical monsoon climate, and leads to a prominent seasonal pattern of tide gate operation. In the dry season (October to March of the coming year), the tide gate remains closed most of the time, and the monthly accumulated opening time amounts to 0.5–2 days with an opening frequency of 5–-14 events/month, while it reaches 5–6 days in the flood season (May to July) with an opening frequency of 19–26 events/month (Table S1).

The tide gate at HMB was a large-scale water conservancy project designed to prevent sea water intrusion and improve the storage of freshwater. Since its operation in the 1970s, it has significantly reduced the salty water intrusion on >300,000 acres of farmland, effectively improved the irrigation of 187,000 acres of farmland and supplied water for domestic and industrial uses for >1,000,000 people. Despite these benefits to local development, the wetland ecosystems of Lianjiang Estuary have been significantly changed (Zhao et al., 2020). Moreover, the high population density in the basin and the unregulated development of textile and dyeing industry along the river resulted in pollution loads exceeding the ecological capacity. This study focused on the highly polluted lower stretch of Lianjiang River between Linbadu Bridge (LB) and the tide gate at HMB. The river discharge and the water quality showed both strong seasonal and interannual variations, due to the collective influence of storm events, treated wastewater effluent, agricultural and fishery releases and tide gate control.

2.2. Sampling campaigns and chemical analyses

Water samples were collected daily at 4 equidistant locations (LB, HP, ZG, HMB) in the lower stretch of Lianjiang River daily from July 23rd to December 30th in 2020. The closed-tide gate period (September 21st to December 30th, 2020) was one of the driest and lowest flow periods of record for the study area, during which nearly no rainfall (7.7 mm) events were recorded. Therefore, the regional WWTP effluents became an important input to the river discharge, and the daily input accounted for 1.36 % of the total river volume in average. During this period, the mixing of the river water with seawater was almost completely blocked, providing an ideal low-flow condition for in-situ examination of the N biotransformation.

Water samples were collected 1.0 m below the surface with a 2-L plexiglass sampler, acidified with H_2SO_4 to pH ≤ 2 and immediately stored in a cooler at 4 °C as per the China National Standard (HJ493-2009) for sample preservation. All samples were delivered to the laboratory within 24 h for filtration and chemical analyses. Total nitrogen (TN), ammonia nitrogen (NH_4^+-N), nitrate nitrogen (NO_3^--N), nitrite nitrogen (NO_2^--N) and Chlorophyll-a (Chl-a) in water samples were measured using spectrophotometric methods, according to China National Standards, i.e., HJ 636-2012, HJ 535-2009, HJ/T 346-2007, GB 7493-1987, and HJ 897-2017, respectively.

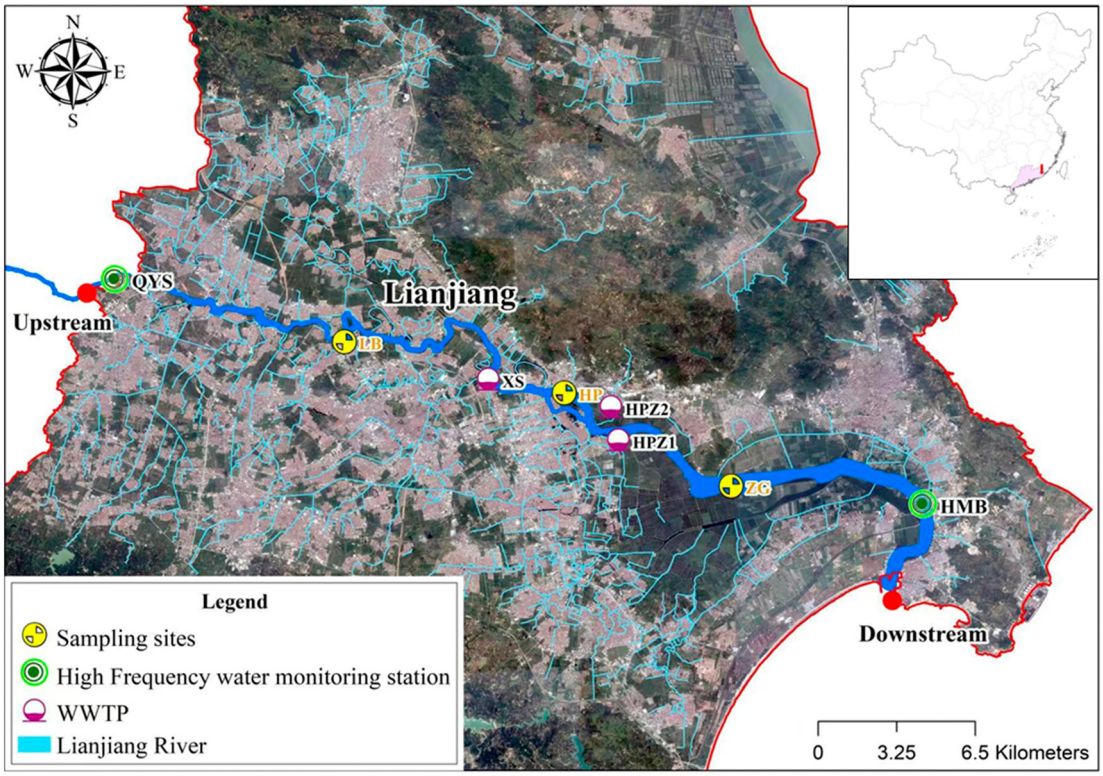

Fig. 1. The study area and the sampling sites.

Within the study region, three WWTPs (XS, HPZ1 and HPZ2) discharge different amounts of treated sewage into the river at separate locations. Sites HP and ZG were located close to the discharge points of the WWTPs. The daily effluent discharge data were collected from the WWTPs, and the N species in the effluent were assumed to be just meeting the national discharge standard for municipal WWTPs (GB18918-2002), i.e., 15 mg·L^{-1} of TN and 10 mg·L^{-1} of NO_3^--N.

2.3. On-line data collection and processing

Online water quality monitoring data were collected from two water monitoring stations: one at HMB, 0.04 km upstream from the tide gate, and the other at QYS, 12.20 km upstream from LB. The water quality monitoring stations monitored velocity and river discharge; recorded temperature, turbidity, specific conductivity, dissolved oxygen and pH hourly; and analyzed TN and NH_4^+-N once every 4 h, using the persulfate digestion method (HJ 636-2012) and the salicylate/hypochlorite colorimetric method (HJ 536-2009), respectively.

The weekly variations of river discharge and NH_4^+-N concentration were quantified in term of the coefficient of variation (CV) according to the following equation:

$$CV = \frac{RMSE}{C_{mean}} \quad (1)$$

where RMSE is the root mean square error of the 4 h^{-1} resolution NH_4^+-N concentrations or river discharges within one week ($n = 42$), while C_{mean} is the mean NH_4^+-N concentration or river discharge in that week.

To elucidate the hydrological impacts on NH_4^+-N dynamics, the NH_4^+-N -discharge hysteresis patterns and metrics were analyzed using the 1-h^{-1} resolution discharge and NH_4^+-N data from the water monitoring station in QYS. The storm events leading to a maximum discharge increase of >20 × 10^4 $m^3 \cdot h^{-1}$ (55.56 $m^3 \cdot s^{-1}$) and a subsequent decrease of at least 50 % compared to the discharge peak were selected. The starting time of a storm event was defined as the first moment when a 10 % increase in discharge was recorded (Rozemeijer et al., 2010). The discharge peaks were merged into one storm event if they occurred within 6 h.

The NH_4^+-N concentration-discharge (C-Q) curves were plotted for the selected storms to characterize their hysteresis behavior, i.e., their direction or rotation patterns. The difference in the mean NH_4^+-N concentration between the rising and falling limbs of the C-Q curves, i.e., the hysteresis index (HI), was determined based on the method of Lloyd et al. (2016). A positive HI indicates clockwise direction of the hysteresis loop, whereas a negative value suggests anticlockwise direction. The slope of the C-Q hysteresis curve is quantified by the relative change in NH_4^+-N concentrations (ΔC) according to the following equation (Butturini et al., 2008):

$$\Delta C = \frac{C_{q,peak} - C_{base}}{C_{max}} \quad (2)$$

where $C_{q,peak}$ is the NH_4^+-N concentration at the peak discharge, C_{base} is the NH_4^+-N concentration at baseflow before the storm, and C_{max} is the maximal NH_4^+-N concentration in the storm. A positive ΔC indicates the solute flushing effect of a storm, whereas a negative ΔC reflects solute dilution.

2.4. Quantification of NO_3^--N transformation

The rate of change in NO_3^--N concentrations in three sections of the river divided by sampling sites, i.e., LB-HP, HP-ZG and ZG-HMB, was calculated using the daily grab water sampling data. In the study section, river discharge was not measured, which made it difficult to determine the fluxes. Therefore, instead of calculating the fluxes, we decided to use the concentration-based travel time model (Jarvie et al., 2018; Kraus et al., 2017) to analyze the removal of NO_3^--N along the river, based on the following facts and assumptions: 1) during the closed-tide gate period, the river discharge was maintained at the base flow, which was almost constant; 2) the daily input (water volume) of treated wastewater effluent accounted for 1.36 % of the total river volume in average, therefore, the river discharge change due to additional wastewater effluent could be negligible; and 3) the N species carried from the treated wastewater effluent

were assumed to undergo no biochemical reactions or assimilatory uptake within the river section that received the effluent. They were subjected to biotransformation and assimilatory uptake in the following section.

The Environmental Fluid Dynamics Code (EFDC) model version 7.1 (Hamrick, 1992) was applied to simulate the flow in the river for the whole dry season of the study year, as detailed previously by Zhao et al. (2020). Briefly, the river was divided into 3D calculation cells, with a spatial resolution ranging from 100 to 300 m in the horizontal direction and 5 layers in the vertical direction in the sigma coordinate, and the flow velocity in each cell was calculated at a resolution of once every 8 h. From this, the average velocity of each section (LB-HP, HP-ZG and ZG-HMB) was determined at the same resolution. The density distribution plot (Fig. S1) of the average velocities showed a log-normal distribution, indicating that low baseflow dominated over the dry season. For simplicity of calculation, the overall average velocity across the closed-tide gate period was determined for each section. Then, the average travelling time of the simulated water parcel was determined to be 3.48 days, 2.00 days and 2.53 days for the section LB-HP, HP-ZG and ZG-HMB, respectively.

The change in NO_3^--N concentration within a section was calculated as the difference between the NO_3^--N concentration in a water parcel out of the section at time t_2 and the initial NO_3^--N concentration in the parcel travelling into the section at time t_1, as shown in Eq. 3.

$$\left[\Delta NO_3^-\right]_{Upper-Lower} = [NO_3]_{Lower}^{t_2} - [NO_3]_{Upper}^{t_1} \quad (3)$$

The apparent rate of change in NO_3^--N concentration per day ($mg{\cdot}L^{-1}{\cdot}d^{-1}$) was then obtained from Eq. 4:

$$R_{NO_3^-} = \frac{\left[\Delta NO_3^-\right]_{Upper-Lower}}{t_2 - t_1} \quad (4)$$

where $t_2 - t_1$ is the water parcel travelling time as aforementioned. Similarly, the apparent rate of change in TN concentration per day ($mg{\cdot}L^{-1}{\cdot}d^{-1}$) was calculated using Eq. 5. Both $R_{NO_3^-}$ and R_{TN} of the three sections were calculated once every day for the closed-tide period, using the daily grab water sampling results.

$$R_{TN} = \frac{[\Delta TN]_{Upper\ -\ Lower}}{t_2\ -\ t_1} \quad (5)$$

The important processes affecting the daily NO_3^--N change rate in the river include the input from WWTPs, removal via denitrification, and assimilatory uptake via photosynthesis. Hence, the overall mass balance of NO_3^--N was calculated according to Eq. 6:

$$R_{NO_3^-} = R_{EFF} + R_{Nitrif} - R_{Denitrif} - R_{Uptake} \quad (6)$$

where R_{EFF} is the rate of NO_3^--N input from WWTPs effluents, R_{Nitrif} is the nitrification rate, $R_{Denitrif}$ is the NO_3^--N removal rate via denitrification, R_{Uptake} is the assimilatory NO_3^--N uptake rate due to photosynthesis. As described above, the daily WWTPs effluents contributed merely 1.36 % of the total river discharge, but introduced a considerable amount of NO_3^--N due to the relatively higher concentration of NO_3^--N. From the equation, the net effect of microbial nitrification and denitrification ($R_{Nitrif} - R_{Denitrif}$) could be quantified.

2.5. Determination of the assimilatory NO_3^--N uptake rate

This study obtained a regressed equation correlating the assimilatory NO_3^--N uptake rate with the concentration of chlorophyll-a using the grab water sampling data at HMB and extrapolated it to other sites. To estimate the assimilatory NO_3^--N uptake rate at HMB, the diurnal dissolved oxygen (DO) curves were analyzed to quantify the DO production rate due to primary production, which was associated with assimilatory NO_3^--N uptake via a stoichiometric equation of photosynthesis and respiration. The details are as follows.

The Delta method, which can be used to estimate photosynthesis, respiration and reaeration in a river system where oxygen deficit dose not vary spatially, was adopted to calculate the DO production rate due to autotrophic primary production. The Delta method gives a piecewise analytical solution of oxygen deficit based on mass balance of DO in conjunction with on-line measurements (Chapra and di Toro, 1991). The DO mass balance was analyzed according to Eq. 7.

$$dD/dt + k_a D = ER_{av} - GPP_{av}(t) \quad (7)$$

where, D is the DO deficit ($mg{\cdot}L^{-1}$), t is the time (d), k_a is the reaeration coefficient (d^{-1}), ER_{av} is the average DO consumption rate due to microalgal respiration ($mg{\cdot}L^{-1}{\cdot}d^{-1}$), and GPP_{av} is the average DO input rate due to gross primary production ($mg{\cdot}L^{-1}{\cdot}d^{-1}$).

The hourly DO on-line monitoring data in HMB were used to calculate the reaeration coefficient (k_a) using the empirical curve (Figs. S2 & S3) obtained by Chapra and di Toro (1991). After screening out low-quality DO data, the remaining data were clustered into three groups according to the time lag between the maximum DO and solar noon (Φ): 1.5 h (n = 11), 2.5 h (n = 7), 3.5 h (n = 9). Then, the average DO input rate due to gross primary production (GPP_{av}) was determined according to the Eq. 8 (Chapra and di Toro, 1991). Where Δ is the diurnal oxygen range; T is the duration of a diurnal cycle (24 h), and f is the duration of photoperiod.

$$\frac{\Delta}{GPP_{av}(t)} \cong \begin{cases} T - f + 0.2\left(\dfrac{f}{T}\right)^2 & \left(k_a \le 1.0\ d^{-1}\right) \\ \dfrac{\left(1-e^{-0.5k_a}\right)^2}{0.5k_a\left(1-e^{-k_a}\right)} + 0.0511 & \left(1.0\ d^{-1} < k_a \le 5.0\ d^{-1}\right) \\ \dfrac{\pi}{\sqrt{k_a^2 + (2\pi)^2}} & \left(k_a > 5.0\ d^{-1}\right) \end{cases} \quad (8)$$

According to previous studies (Hall and Tank, 2003; Jarvie et al., 2018), around 50 % of the DO input from microalgal photosynthesis would be consumed by microalgal respiration. Therefore, the obtained values of GPP_{av} were converted into the DO input rate due to net primary production (NPP), assuming that autotrophic respiration consumed 50 % of the GPP_{av}. Based on the stoichiometric equation (Eq. 9) of microalgal photosynthesis and respiration in the fresh water (Stumm and Morgan, 1996), NPP was converted into the assimilatory NO_3^--N uptake rate (R_{Uptake}) according to Eq. 10.

$$106CO_2 + 16HNO_3 + H_3PO_4 + 122H_2O \leftrightarrow (CH_2O)_{106}(NH_3)_{16}H_3PO_4 + 138O_2 \quad (9)$$

$$R_{Uptake} = \frac{7}{138}\ NPP_{av} \quad (10)$$

From this, a linear regression ($R^2 = 0.9148$) could be fitted into the curve of R_{Uptake} vs chlorophyll-a (Chl-a) obtained at HMB (Eq. 11), which was applied to other sites due to the short distance between each site.

$$R_{Uptake} = 0.0042 \times Chl - \alpha + 0.0841 \quad (11)$$

2.6. Statistical analysis

The two-way ANOVA and Fisher's LSD tests were conducted to reveal the significance of differences using the software Origin.

3. Results

3.1. Dynamics of rainfall, river charge and NH_4^+-N indicated from the on-line monitoring data

The rainfall intensity in the area was 1156.8 mm in the survey year (2020) with a total of 25 rainfall events (Fig. 2a). The primary rainfall

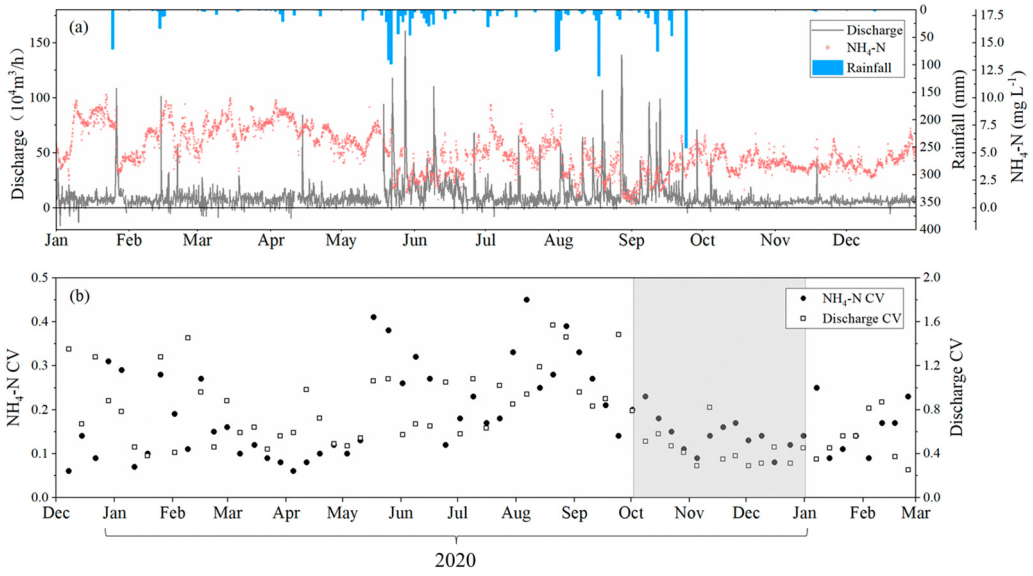

Fig. 2. The daily NH_4^+-N concentration, rainfall intensity, and the 2-h river discharge of year 2020 recorded at QYS on-line monitoring station (a), and the coefficient of variations of NH_4^+-N and river discharge on a weekly basis (b). The grey shadow represents the closed-tide gate period.

events occurred in August, May, September, and April with monthly rainfall of 347.5 mm, 245.8 mm, 160.4 mm and 144.5 mm, respectively. The least monthly rainfall (3.0 mm) was recorded in October. Within the year, 22 days showed a daily rainfall intensity >20 mm.

The river discharge ranged from -21.38 to 161.04×10^4 $m^3 \cdot h^{-1}$, with the base flow fluctuated around 25×10^4 $m^3 \cdot h^{-1}$. Compared to other seasons, more river discharge peaks were observed in summer (June–August) and mainly in August, while the largest discharge of 161.04×10^4 $m^3 \cdot h^{-1}$ occurred in May.

The NH_4^+-N concentrations also showed a large variation from 0.33 $mg \cdot L^{-1}$ to 12.79 $mg \cdot L^{-1}$ and averaged 5.51 $mg \cdot L^{-1}$; the mean NH_4^+-N concentrations in winter (December–February, 7.34 mg L^{-1}) and spring (March to May, 6.58 mg L^{-1}) were higher than those in summer (June to August, 4.20 mg L^{-1}) and autumn (September to November, 3.90 mg L^{-1}). The NH_4^+-N concentration fluctuated dramatically with the river discharge during storm events.

The coefficients of variation of the river discharge and NH_4^+-N concentration ranged from 0.25 to 1.57 and 0.06 to 0.45, respectively (Fig. 2b). The tide gate at HMB was typically opened 1–3 days earlier or later than a rainfall event, leading to a river discharge peak inconsistent with the rainfall events. Hence, tide gate regulation rather than rainfall events was the primary factor controlling streamflow in Lianjiang River, resulting in complex and asynchronous variations in NH_4^+-N concentration and river discharge.

The ratio of coefficients of variation (CV) of concentration and discharge, CV_c/CV_q, is widely used to evaluate the relative variability of concentration and discharge. A low CV_c/CV_q value indicates a low variability of concentration, which is termed as chemostatic behavior; while a high CV_c/CV_q value (≥ 0.5) suggests a chemodynamic regime (Knapp et al., 2022). The weekly CV_c (NH_4^+-N)/CV_q values in the study year were in the range of 0.076 to 0.48 with a mean of 0.28, indicating a chemostatic pattern of NH_4^+-N in the upstream section of Liangjiang River.

To further elucidate the impacts of precipitation-induced discharge on NH_4^+-N dynamics, the hysteresis patterns of 15 storm events occurred in 2020 were analyzed (Fig. 3). Among the 15 events, 10 events showed a clockwise hysteresis pattern, indicating a dilution effect ($HI_{mean} > 0$, $\Delta C < 0$) on NH_4^+-N (Table S2), while the remaining 5 events with an anticlockwise hysteresis pattern resulted in an increase in NH_4^+-N with flow, reflecting a nutrient-flushing effect, except the storm on Sep. 24 (Fig. 3o). Noticeably, all the 4 N-flushing anticlockwise hysteresis patterns (Fig. 3c, d, h, and n) occurred at a lower peak discharge range of 25×10^4–70×10^4 $m^3 \cdot h^{-1}$, compared to the typical range of 100×10^4–120×10^4 $m^3 \cdot h^{-1}$ for the clockwise hysteresis patterns. This suggests that the low intensity rainfall would cause the increase in river NH_4^+-N concentrations, while the high intensity rainfall would dilute NH_4^+-N, instead. Two clockwise hysteresis regimes (Fig. 3g and j) had a peak discharge of 60×10^4–70×10^4 $m^3 \cdot h^{-1}$; however, as the second storm events following the first ones immediately, their dilution effects on NH_4^+-N were highly expected.

The C-Q curve on Sep. 24 (Fig. 3o) was the only anticlockwise hysteresis showing a slight dilution effect on NH_4^+-N. This could be attributed to the tide gate regulation, which postponed the discharge peak by 4 days (Table S2) and reduced the influence of flow change on the transport of nutrients from catchment to the stream. There were one- or two-days differences between the discharge and rainfall peaks in other storm events (Fig. 3a, k, and n), however, the hysteresis patterns seemed not to be affected. This suggests that the hysteresis pattern in NH_4^+-N concentration-discharge during storm events was primarily decided by the rainfall intensity, and tide gate regulation might reduce this impact in a few cases when tide gate opening was delayed for a prolonged period (~4 days).

3.2. Variations of TN, NH_4^+-N, NO_3^--N, NO_2^--N and Chl-a in the grab samples

The monthly average water quality data of the grab samples were shown in Table 1. From the late summer (July) to early winter (December), the water temperature at HMB declined from 33.62 °C to 16.20 °C, while the pH values were stable in the range of 7.41 to 8.84. For the grab water samples, seasonal and spatial variations were prominent (Fig. 4). The mean TN concentrations ranged from 2.80 $mg \cdot L^{-1}$ to 7.51 $mg \cdot L^{-1}$ along the river, and the mean in December was higher than other months. The mean NO_3^--N concentrations was in the range of 0.56 $mg \cdot L^{-1}$ to 4.33 $mg \cdot L^{-1}$ showing an increasing order of September < October < November < December ($p < 0.001$), with the highest mean at the upstream site LB. Conversely, the mean NH_4^+-N concentrations declined from 4.55 $mg \cdot L^{-1}$ to 0.38 $mg \cdot L^{-1}$ during the closed-tide gate period (October to December). The mean NO_2^--N concentration was lower than other N species and fluctuated between 0.07 $mg \cdot L^{-1}$ in September and 0.63 $mg \cdot L^{-1}$ in July.

Huge variations were observed for Chl-a concentrations in each month, and the mean Chl-a concentrations ranged from 27.95 $\mu g \cdot L^{-1}$ in July to 81.85 $\mu g \cdot L^{-1}$ in December. In particular, the SD values reached 43.63 $\mu g \cdot L^{-1}$ in August when storm events caused large and rapid fluctuation of stream flow.

There was a clear difference between the rainfall period, characterized by regular storm events from mid-July to late September, and almost no rainfall (merely 7.7 mm) within the closed-tide gate period from October

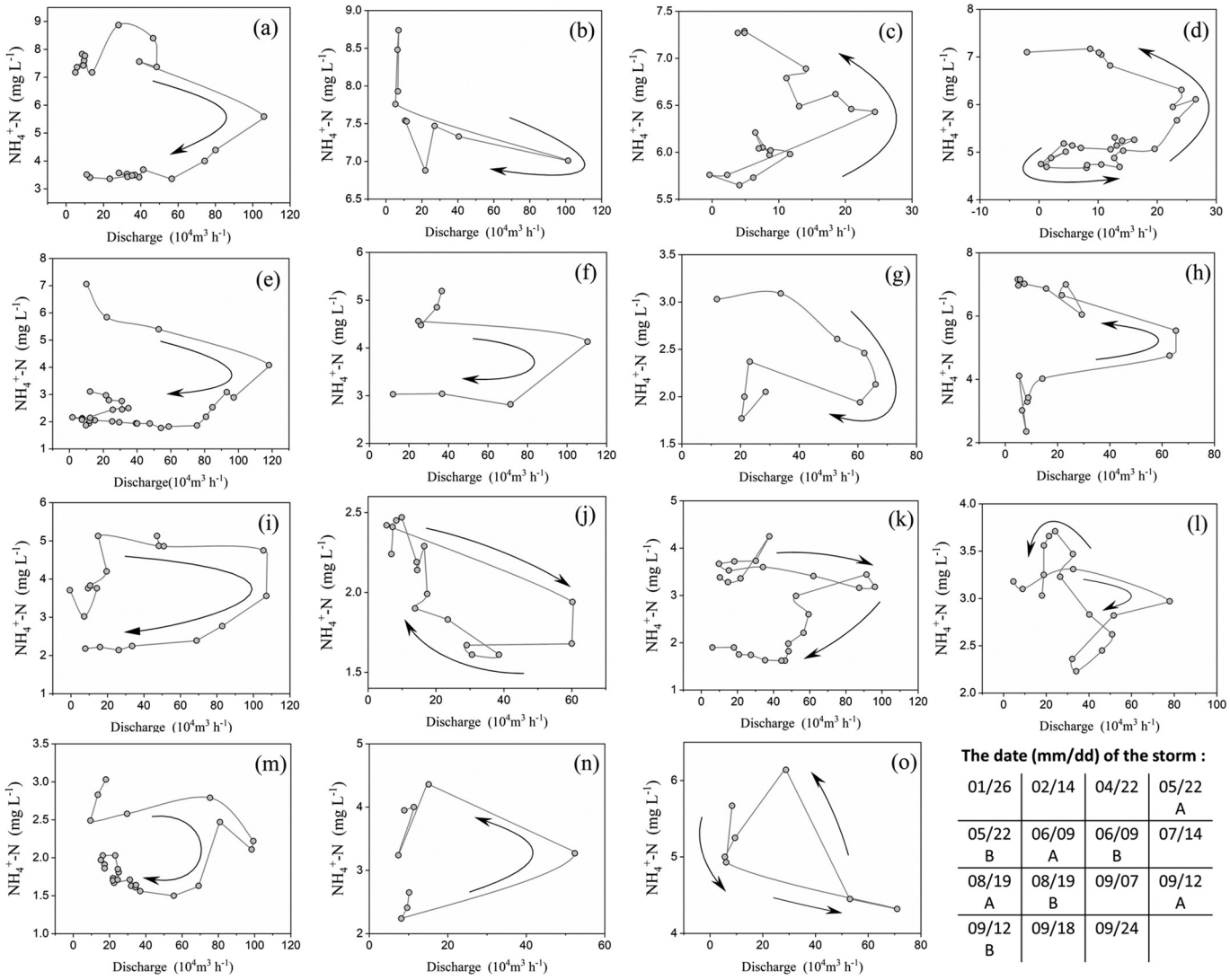

Fig. 3. The hysteresis curves of NH_4^+-N vs discharge of selected storm events occurred in 2020. 'A' and 'B' denotations in the storm event date differentiate the first and second storm events occurred on the same day.

to December (Fig. 4). Spatially, the concentrations of NO_3^--N showed no significant difference in the upstream section between LB and HP (p = 0.767), but a decreasing trend from HP to the downstream sections ($p < 0.001$), i.e., LB = HP > ZG > HMB during the closed-tide gate period. While for other nitrogen species, i.e., TN, NH_4^+-N and NO_2^--N, significant ($p < 0.03$) decreasing patterns from upstream to downstream sections (LB > HP > ZG > HMB) was prominent. No apparent trend in Chl-a concentrations was found at the sample site LB, HP, and ZG, while the mean Chl-a concentrations at HMB tended to be the lowest during the closed-tide gate period (Oct to Dec).

3.3. Removal of N along the river

The major inputs of N to a section were the N conveyed from upstream and WWTPs outfalls in the region. One WWTP was located between sites LB and HP, discharging 8070 m^3 of treated effluent containing approximately 15 $mg{\cdot}L^{-1}$ TN (including 10 $mg{\cdot}L^{-1}$ NO_3^--N) into this section daily, which resulted in an $R_{EFF\,|\,LB-HP}$ of 0.10 $mg{\cdot}L^{-1}{\cdot}d^{-1}$ during the closed-tide gate period. For the section HP-ZG, another two WWTPs discharging 2540 m^3 of treated effluent resulting in an $R_{EFF\,|\,HP-ZG}$ of 0.03 $mg{\cdot}L^{-1}{\cdot}d^{-1}$. As no WWTP outfalls were located between sites ZG and HMB, the input of WWTP effluent was null in this section.

During the closed-tide gate period, a clear elevation in NO_3^--N concentrations in conjunction with a decrease in NH_4^+-N concentrations was observed. From Eq. 4, the rate of change in NO_3^--N concentrations within the two adjacent sampling sites was determined. As shown in Table 2, the net rate of change in NO_3^--N between LB and HP ($R_{NO_3^-\,|\,LB-HP}$) was positive in the early stage (Sep. to Oct.) of the closed-tide gate period, but turned negative afterwards; while the other sections showed negative $R_{NO_3^-}$ values within the whole study period, indicating the increasing NO_3^--N removal along the river. This is most prominent for the middle section HP-ZG.

The TN removal rate (R_{TN}) ranged from -0.12 $mg{\cdot}L^{-1}{\cdot}d^{-1}$ to -1.14 $mg{\cdot}L^{-1}{\cdot}d^{-1}$ along the river, and it seemed not to be significantly ($p > 0.10$) affected by months. Along the river, the middle section (HP-ZG) had the largest TN removal rate, while the upstream and downstream sections (LB-HP and ZG-HMB) showed similar rates (p = 0.26). Most of the time, R_{TN} was negative, indicating the removal of TN along the river, although positive values occurred in a few cases most probably due to unpredictable inputs, such as fishery or other non-point pollutions within the study period.

3.4. Assimilatory NO_3^--N uptake

Assimilatory NO_3^--N uptake at HMB was determined by the Delta Method as described earlier. During the study period, the time lag between

Table 1
The monthly water quality data of Lianjiang River from July to December 2020. Temperature and pH were recorded from the on-line monitoring station in HMB, while other water quality parameters were from the grab water sampling campaigns. The data were in mean ± standard deviation (SD).

Mon.	Site	Temp. (°C)	pH	TN ($mg{\cdot}L^{-1}$)	NO_3^--N ($mg{\cdot}L^{-1}$)	NO_2^--N ($mg{\cdot}L^{-1}$)	NH_4^+-N ($mg{\cdot}L^{-1}$)	Chl-a ($\mu g{\cdot}L^{-1}$)
Jul.	LB	–	–	6.44 ± 1.13	1.99 ± 0.22	0.65 ± 0.26	3.50 ± 0.39	58.05 ± 33.21
	HP	–	–	6.10 ± 1.70	2.20 ± 0.20	0.64 ± 0.19	2.17 ± 0.27	42.07 ± 15.47
	ZG	–	–	3.84 ± 0.98	2.24 ± 0.37	0.44 ± 0.06	1.07 ± 0.13	50.19 ± 16.51
	HMB	32.49 ± 0.77	7.79 ± 0.50	2.80 ± 0.60	1.65 ± 0.34	0.43 ± 0.11	0.14 ± 0.04	27.95 ± 8.70
Aug.	LB	–	–	5.43 ± 1.47	1.01 ± 0.32	0.08 ± 0.07	4.20 ± 0.59	70.58 ± 43.63
	HP	–	–	5.18 ± 0.90	1.11 ± 0.41	0.13 ± 0.15	3.21 ± 0.64	58.13 ± 33.48
	ZG	–	–	4.87 ± 1.05	0.96 ± 0.42	0.18 ± 0.15	2.88 ± 0.74	76.96 ± 39.28
	HMB	31.20 ± 1.09	7.53 ± 0.51	4.50 ± 0.86	1.02 ± 0.37	0.24 ± 0.14	2.13 ± 0.97	59.40 ± 31.61
Sep.	LB	–	–	4.66 ± 1.55	0.69 ± 0.17	0.06 ± 0.02	3.74 ± 0.83	43.46 ± 24.67
	HP	–	–	4.42 ± 1.92	0.78 ± 0.22	0.07 ± 0.03	3.07 ± 0.63	31.69 ± 14.92
	ZG	–	–	3.93 ± 1.09	0.68 ± 0.28	0.08 ± 0.04	2.80 ± 0.52	46.40 ± 32.97
	HMB	30.42 ± 1.47	7.35 ± 0.48	3.81 ± 1.22	0.56 ± 0.15	0.09 ± 0.03	2.35 ± 0.48	36.14 ± 22.80
Oct.	LB	–	–	6.54 ± 1.07	1.68 ± 0.78	0.38 ± 0.21	4.55 ± 0.50	52.80 ± 16.46
	HP	–	–	5.59 ± 1.30	2.21 ± 0.74	0.43 ± 0.15	3.30 ± 0.49	65.32 ± 41.79
	ZG	–	–	4.34 ± 1.48	1.69 ± 0.45	0.40 ± 0.08	2.62 ± 0.71	53.38 ± 25.17
	HMB	26.29 ± 1.56	7.99 ± 0.29	3.77 ± 0.62	1.01 ± 0.27	0.33 ± 0.08	1.11 ± 0.35	40.71 ± 29.09
Nov.	LB	–	–	6.57 ± 1.00	3.44 ± 0.48	0.45 ± 0.13	3.23 ± 0.33	66.23 ± 38.37
	HP	–	–	5.33 ± 1.03	2.97 ± 0.56	0.33 ± 0.08	2.24 ± 0.22	75.51 ± 34.86
	ZG	–	–	3.14 ± 0.69	1.99 ± 0.38	0.28 ± 0.06	1.61 ± 0.40	59.05 ± 23.33
	HMB	23.51 ± 1.22	7.90 ± 0.40	2.69 ± 0.47	1.24 ± 0.28	0.24 ± 0.05	0.48 ± 0.22	34.15 ± 21.93
Dec.	LB	–	–	7.51 ± 0.63	4.33 ± 0.68	0.50 ± 0.12	2.72 ± 0.29	56.35 ± 28.16
	HP	–	–	6.36 ± 0.53	4.13 ± 0.71	0.33 ± 0.12	1.54 ± 0.22	81.85 ± 35.68
	ZG	–	–	3.97 ± 0.65	2.78 ± 0.46	0.29 ± 0.08	1.28 ± 0.20	72.13 ± 31.68
	HMB	19.46 ± 1.30	7.88 ± 0.20	2.84 ± 0.60	1.74 ± 0.41	0.22 ± 0.05	0.38 ± 0.14	38.72 ± 22.32

the maximum DO and solar noon (Φ) could be categorized into three groups: 1.5 h (11 sampling days), 2.5 h (7 sampling days), and 3.5 h (9 sampling days) (Fig. S4 & Table S3). As shown in Fig. 5, linear regression (R^2 = 0.9148) between R_{Uptake} and Chl-a concentration was obtained for the Φ of 3.5 h, while no linear regression curve could be fitted when all Φ were included. Several unreasonable DO data were obtained for Φ of 1.5 and 2.5 h, which could be caused by many factors, such as fishery and unintentional discharge from agricultures. This result corresponds well with the study of Chapra and di Toro (1991), who determined a Φ of 3.93 h.

The linear regression between GPP_{AV} and Chl-a concentrations was applied to other sites, from which the average NO_3^--N uptake rate of the two adjacent sites was determined as the assimilatory NO_3^--N uptake of the section between the two sites. Fig. 6a shows the variation of daily R_{Uptake} in different sections during the closed-tide period, which followed a general increasing trend with time from September to late November. In December, huge variations in the daily R_{Uptake} were observed, and two rapid rising cycles were prominent. This corresponds well with the Chl-a concentration in the rive (Fig. 4e). Among the three sections, the downstream section ZG-HMB showed a considerably lower R_{Uptake} than the other two upstream sections. To better compare the results, the monthly averaged R_{Uptake} was summarized in Table 2; the range of monthly averaged R_{Uptake} was from 0.18 ± 0.06 $mg{\cdot}L^{-1}{\cdot}d^{-1}$ in ZG-HMB in September to 0.40 ± 0.12 $mg{\cdot}L^{-1}{\cdot}d^{-1}$ in HP-ZG in December. A gradual increase in R_{Uptake} with time (from September to December) and a decrease from upstream to downstream was prominent, which is similar to the trend of TN removal. From Table 2, the daily assimilated proportion of nitrogen was determined to be 40 %–75 % of the total nitrogen removal, indicating the important role of assimilatory uptake of nitrate in Lianjiang River during the closed-tide gate period.

3.5. NO_3^--N transformation

In the study region, nitrification and denitrification were the two major processes governing NO_3^--N transformation in the river in addition to assimilatory NO_3^--N uptake by algae. Nitrification is a two-step process involving the first oxidation of NH_4^+-N to NO_2^--N and then to NO_3^--N. Both steps are affected by numerous environmental factors, which makes it difficult to quantify the rates. Therefore, the overall effect of nitrification and denitrification was evaluated by comparing the difference between R_{Nitrif} and $R_{Denitrif}$.

As shown in Table 2 & Fig. 6b, positive values of $R_{Nitrif} - R_{Denitrif}$ were recorded for all three sections in September and October, with a decreasing trend from upstream to downstream, suggesting the dominance of nitrification in the upstream section of the river. In November and December, $R_{Nitrif} - R_{Denitrif}$ turned to negative values in HP-ZG and ZG-HMB, indicating the dominance of denitrification in the downstream section in winter. Noticeably, $R_{Nitrif} - R_{Denitrif}$ in HP-ZG showed much greater absolute values than that in ZG-HMB, which always had the least $R_{Nitrif} - R_{Denitrif}$ value. Therefore, nitrification and denitrification seemed to reach a steady state in the lowermost section of Lianjiang River.

The TN removal rate (Fig. 6c) showed a similar trend with $R_{Nitrif} - R_{Denitrif}$, and both corresponded well with the NO_3^--N concentration profiles. For example, NO_3^--N concentrations gradually increased from 0.42 $mg{\cdot}L^{-1}$ to 5.35 $mg{\cdot}L^{-1}$ from September to December at HP. Meanwhile R_{TN} in the section HP-ZG increased from 0.52 ± 0.15 to 1.20 ± 0.17 $mg{\cdot}L^{-1}{\cdot}d^{-1}$, and $R_{Nitrif} - R_{Denitrif}$ was decreased from 0.10 ± 0.11 to −0.26 ± 0.26 $mg{\cdot}L^{-1}{\cdot}d^{-1}$. This suggests that the total nitrogen removal and the denitrification rate were largely affected by the substrate (NO_3^--N) concentration.

From October to December, the NH_4^+-N concentration declined from 5.34 $mg{\cdot}L^{-1}$ to 2.18 $mg{\cdot}L^{-1}$ at the site LB, where the highest NH_4^+-N concentration was recorded. The section LB-HP had the highest $R_{Nitrif} - R_{Denitrif}$ in October (0.43 ± 0.12 $mg{\cdot}L^{-1}{\cdot}d^{-1}$), indicating the advantage of nitrification over denitrification. Comparing with upstream sites, the downstream site HMB had the lowest NH_4^+-N and NO_3^--N concentrations, and also the lowest absolute value of $R_{Nitrif} - R_{Denitrif}$ in section ZG-HMB, suggesting that nitrification was also primarily dependent on the substrate (NH_4^+-N) concentration. Therefore, the rates of both denitrification and nitrification in Lianjiang River were highly limited by the substrate concentration.

4. Discussion

4.1. Impacts of hydrological and biogeochemical processes on N dynamics

The chemostatic pattern of NH_4^+-N in the upstream section of Lianjiang River infers the homogenous distribution of NH_4^+-N in the watershed so that precipitation-induced discharge changes did not result in significant changes in solute concentrations (Fazekas et al., 2020). Similar chemostatic

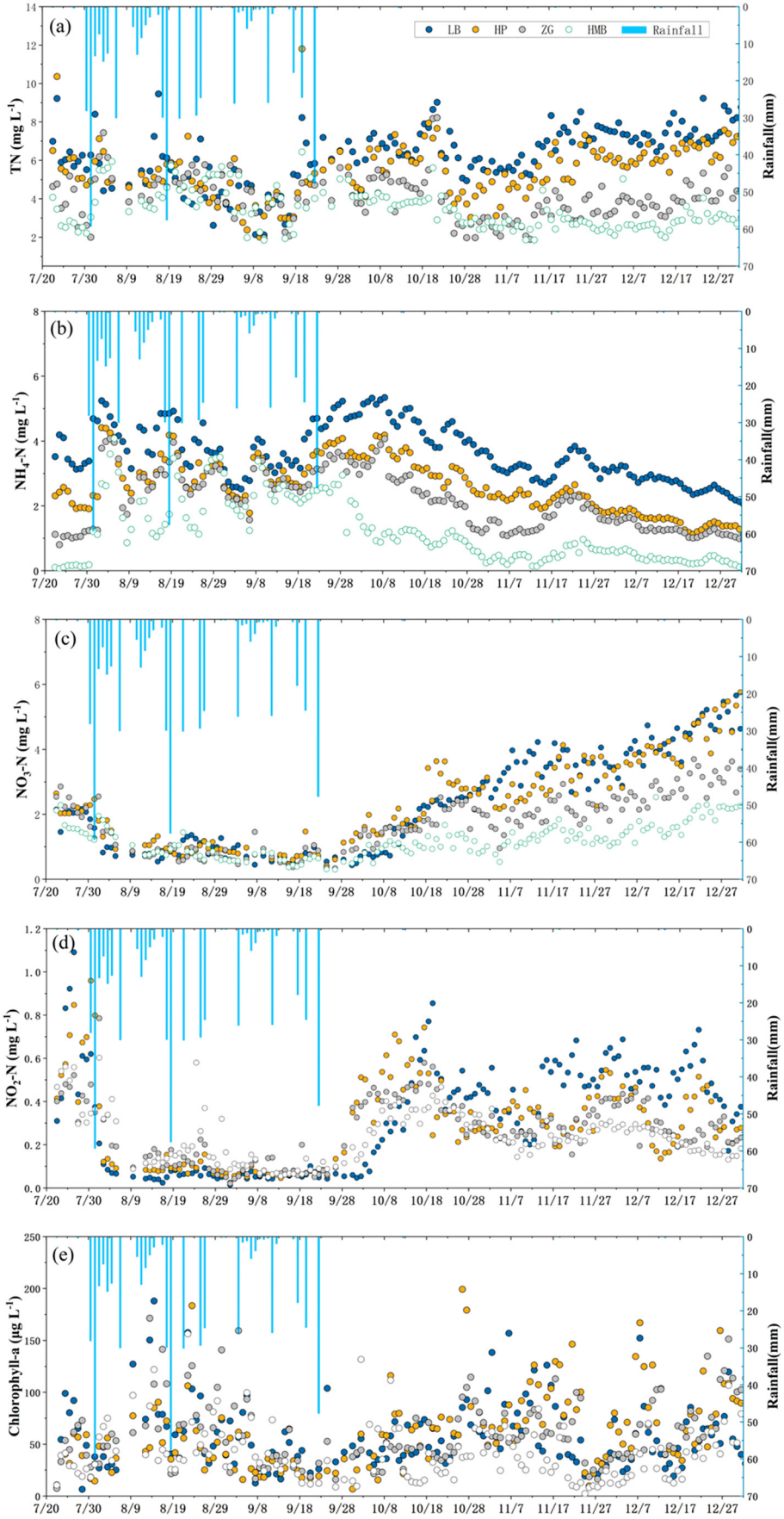

Fig. 4. The daily water quality data from the grab water sampling; (a) TN, (b) NH_4^+-N, (c) NO_3^--N, (d) NO_2^--N, and (e) Chlorophyll-a from July 23rd to December 30th.

Table 2
The input and biotransformation rates of NO_3^--N, and the total removal rate of NO_3^--N and TN in the three sections (LB-HP, HP-ZG, ZG-HMB) in Lianjiang River (unit: $mg{\cdot}L^{-1}{\cdot}d^{-1}$).

Month	Section	Rate of processes affecting NO_3^--N			$R_{NO_3^-}$	R_{TN}
		R_{EFF}	R_{Uptake}	$R_{Nitrif} - R_{Denitrif}$		
Sep.	LB-HP	0.13 ± 0.015	0.25 ± 0.08	0.10 ± 0.19	0.12 ± 0.10	−0.21 ± 0.25
	HP-ZG	0.05 ± 0.001	0.21 ± 0.04	0.10 ± 0.12	−0.06 ± 0.13	−0.46 ± 0.30
	ZG-HMB	–	0.18 ± 0.06	0.12 ± 0.16	−0.06 ± 0.14	−0.12 ± 0.38
Oct.	LB-HP	0.10 ± 0.011	0.33 ± 0.11	0.43 ± 0.14	0.20 ± 0.13	−0.32 ± 0.52
	HP-ZG	0.03 ± 0.010	0.33 ± 0.13	0.07 ± 0.25	−0.23 ± 0.26	−0.68 ± 0.56
	ZG-HMB	–	0.28 ± 0.09	0.02 ± 0.16	−0.26 ± 0.16	−0.30 ± 0.51
Nov.	LB-HP	0.09 ± 0.009	0.38 ± 0.13	0.17 ± 0.20	−0.12 ± 0.18	−0.31 ± 0.26
	HP-ZG	0.04 ± 0.004	0.37 ± 0.12	−0.10 ± 0.36	−0.43 ± 0.34	−1.09 ± 0.48
	ZG-HMB	–	0.28 ± 0.08	−0.02 ± 0.19	−0.30 ± 0.17	−0.18 ± 0.32
Dec.	LB-HP	0.100 ± 0.008	0.37 ± 0.12	0.27 ± 0.17	0.01 ± 0.13	−0.29 ± 0.24
	HP-ZG	0.04 ± 0.003	0.40 ± 0.12	−0.26 ± 0.26	−0.62 ± 0.30	−1.14 ± 0.35
	ZG-HMB	–	0.31 ± 0.11	−0.07 ± 0.18	−0.38 ± 0.15	−0.40 ± 0.27

patterns have been observed for dissolved organic carbon, nutrients, and weathering products (Burns et al., 2019).

The hysteresis patterns of storm events reflect the complex influences of internal (e.g., soils and land use) and external (e.g., precipitation intensity) factors on C-Q relationships. Clockwise hysteresis in nutrient concentrations is generally observed for urban watersheds, where dilution of nutrients from point sources (e.g., combined sewer overflow and WWTP effluent outfalls) often occur, with a short-lived spike as the precedent in some cases (Burns et al., 2019). In contrast, the high nutrient content in agricultural land could be sustained in short-term precipitation, and typically results in a rise in the stream nutrient concentration during a storm, reflecting a nutrient flushing effect (Blaen et al., 2016; Jones et al., 2017). Both clockwise and anticlockwise hysteresis patterns in NH_4^+-N have been observed in this study, with the majority (10 out of 15) showing the dilution effect, indicating the significance of point sources in NH_4^+-N load to the river. However, considering the mixed land use in Lianjiang River catchment, transport of NH_4^+-N from agricultural sources cannot be ignored. Other than the land type, rainfall intensity seems to be a more principal factor deciding the hysteresis patterns of NH_4^+-N in storm events.

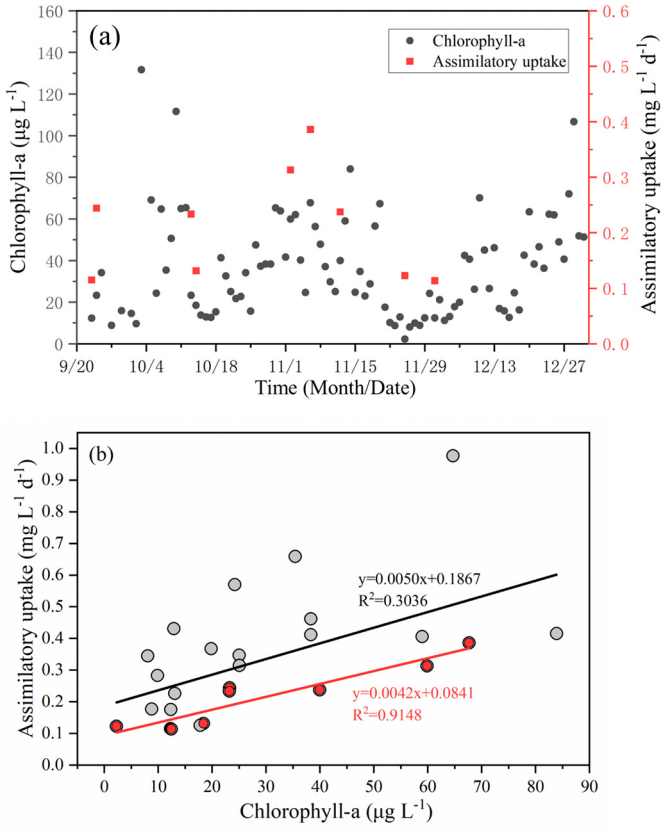

Fig. 5. The assimilatory NO_3^--N uptake rates and Chl-a concentrations at site HMB during the closed-tide gate period (a) and their linear regression (b). Only the uptake rates of the 3.5-h Φ were shown in (a); the black linear regression curve was for all Φ, while the red was only for the 3.5-h Φ.

The grab water sampling from the downstream sections suggests a clear decreasing trend in NH_4^+-N concentrations with time in the dry season accompanied by an increase in NO_3^--N concentrations. Compared with the wet season, a significantly higher level of NO_2^--N was maintained relatively consistently in the dry season. As the upstream input of N species was almost constant, this seasonality in N species in the downstream sections could be most probably attributed to biogeochemical processes occurring in the river. The tide gate regulation scheme, i.e., opening for a brief period at a low frequency, sustained the least variation in hydrological conditions in the dry season, thus facilitating the biogeochemical transformation of N species along the river.

4.2. Effects of assimilatory uptake by phytoplankton on nitrate

The assimilatory nitrate uptake accounts for different fractions of the total nitrate flux in streams depending on the type of phytoplankton. For example, the assimilatory portion of nitrate by diatoms could amount to 30 % in a river during the low flow period (House et al., 2001). Nitrate assimilation by plants accounted for 40 to 70 % of the measured nitrogen flux in streams (Jansson et al., 1994). Macrophytes and algae in streams could contribute to >40 % of the total nitrogen removal via assimilation, although with huge uncertainties (Birgand et al., 2007). In another study, phytoplankton nitrate assimilation accounted for two-thirds of the total nitrate flux (Triska et al., 1983). The daily assimilated proportion of nitrogen in this study was about 40 %–75 %, which agrees well with the reported studies, indicating the important role of phytoplankton in assimilatory uptake of nitrate in Lianjiang River.

The estimated assimilatory NO_3^--N uptake rate (R_{Uptake}) clearly indicates an increasing trend with time (Sep. to Dec.) during the closed-tide gate period in this study. Temperature is often acknowledged as one of the key factors affecting assimilation of phytoplankton. Zhao et al. (2019) showed that phytoplankton uptake rate was almost linearly increased with temperature from ~12.5 °C until 27.9 °C. While our study showed that the mean R_{Uptake} increased from October to December with a decrease in temperature from 26.29 °C to 19.46 °C, indicating that factors other than temperature, e.g., the NO_3^--N concentration and clarity, also played important roles in regulating phytoplankton growth in Lianjiang River.

The daily assimilatory NO_3^--N uptake per Chl-a of this study ($0.0042\ mg{\cdot}\mu g^{-1}{\cdot}d^{-1}$) is similar to the half-saturation constant of assimilatory N uptake of algae per Chl-a ($0.0050\ mg{\cdot}\mu g^{-1}{\cdot}d^{-1}$) in Taihu Lake, China, as determined by Zhao et al. (2019). This suggests that the low discharge and high clarity conditions within the closed-tide gate period, have

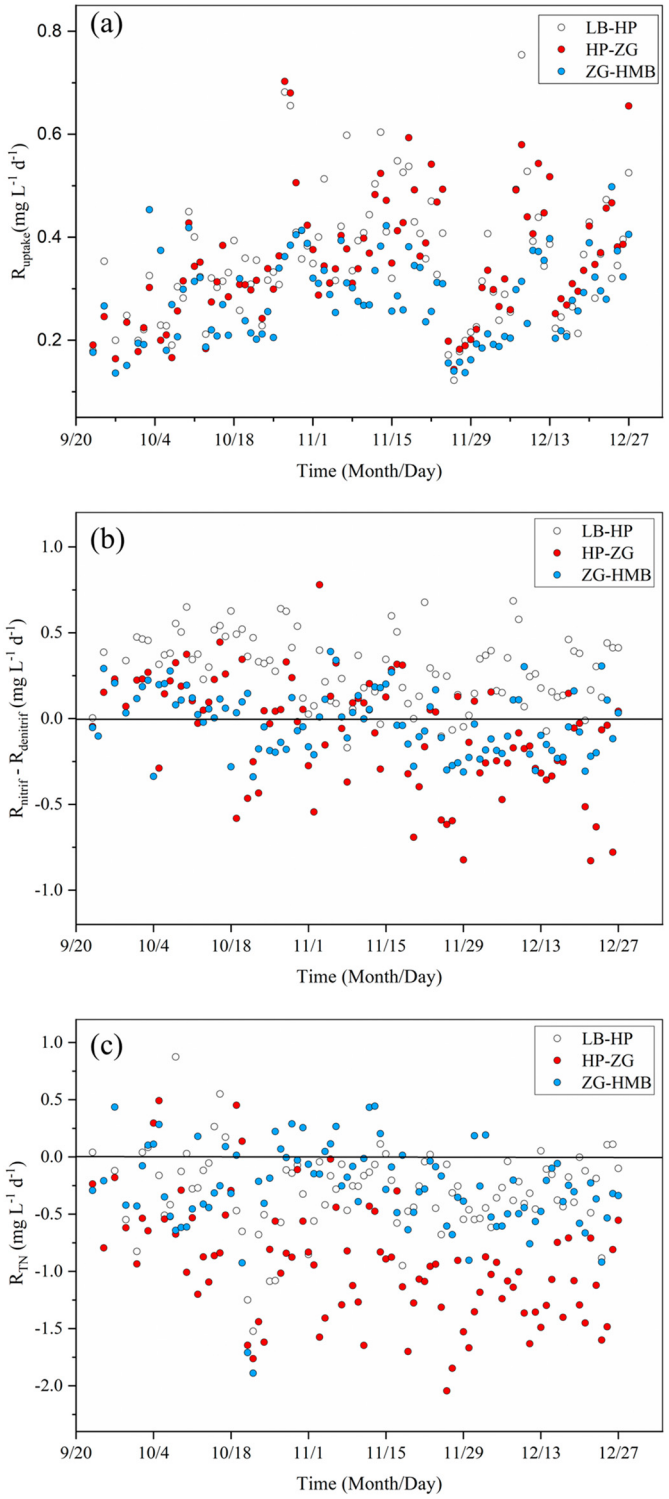

Fig. 6. The rates of (a) assimilatory NO_3^--N uptake, (b) nitrification-denitrification, and (c) TN removal, in different sections of Lianjiang River during the closed-tide gate period.

favored the growth of microalgae and rendered the lower section of Lianjiang River a phytoplanktonic growth environment similar to shallow lakes.

In our study, we applied an alternative approach integrating Chl-a data estimated from grab water sampling and assimilatory NO_3^--N uptake rate determined from continuous DO monitoring data to estimate daily assimilatory NO_3^--N uptake rate along the river. It shows that for long-term phytoplankton effect in large-scale river systems, combination of on-line water monitoring and grab water sampling may provide more reliable data for dynamic phytoplankton studies.

4.3. Net effects of nitrification-denitrification

From upstream (LB) to downstream (HMB), a gradual decline in the monitored N species (NO_3^--N, NH_4^+-N and TN) was observed, suggesting that a significant amount of nitrogen was removed from the river. During the closed-tide gate period, no rainfall events occurred, and thus non-point source pollution was negligible; N transport from upstream became the sole N input to the river. In the early stage of the closed-tide gate period, the highest $R_{Nitrif} - R_{Denitrif}$ in the upper section LB-HP with the highest NH_4^+-N concentration was observed, suggesting the dominance of nitrification in this section. While denitrification became dominant in the middle section HP-ZG, thus contributing to significant removal of N from the river. With the decrease in substrate concentrations, the lowest $R_{Nitrif} - R_{Denitrif}$ was recorded in the downstream section ZG-HMB. Moreover, the increase in NO_3^--N concentrations and the decrease in NH_4^+-N concentrations were also observed in the upstream section of QYS. Therefore, the net nitrification-denitrification effect has resulted in the gradual increase in nitrogen removal with time in Lianjiang River during the closed-tide gate period.

The net effect of nitrification-denitrification depends on temperature and the ratio of NO_3^--N/NH_4^+-N (Zheng et al., 2016). Previous studies in another subtropic river in South China — Pearl River indicated that the water temperature was high enough in December to sustain significant denitrification (Chen et al., 2009). Both rates of denitrification and nitrification in rivers are highly dependent on the substrate concentration. For example, the study by van Kessel (1977) showed an almost linear relationship between the denitrification rate and NO_3^--N concentration. Risgaard-Petersen et al. (1998) used an isotope pairing technique to trace N_2 produced by denitrification in sediments and concluded the relative contribution of denitrification was dependent on the nitrate concentrations in the water column. In addition, water residence time is also an important factor, as a longer residence time in winter (dry season) resulted in a greater nitrification extent compared to that in summer (wet season) in Pearl River (Ye et al., 2016). The closed-tide period in Lianjiang River has facilitated the development of both nitrification and denitrification along the river and with time. As a consequence, greater N removal was observed in December than in September.

Previous studies have shown that denitrification contributed to a significant amount of the total riverine N removal, e.g., >50 % (Ator and Garcia, 2016; Zhang et al., 2019) or 37 % (van Breemen et al., 2002) or 47 %–65 % (Hill and Sanmugadas, 1985). The rate of denitrification ($R_{Denitrif}$) was difficult to be estimated by grab water sampling due to its strong interaction with benthic sediments in this study. However, as fixation of nitrogen by micro phytoplankton could be neglected over the long study period, the rate of TN removal (R_{TN}) may represent the rate of denitrification.

5. Conclusion

Daily grab water sampling and on-line water monitoring were combined to investigate the spatiotemporal variations in N species in the tide gate-regulated Lianjiang River, and to elucidate the extent of nitrate transformation during the closed-tide gate period. The major conclusions are as follows.

1) The NH_4^+-N concentrations were chemostatic in the upstream section of Lianjiang River showing prominent seasonality. The flushing or dilution effect of a storm event on N species was primarily decided by the rainfall intensity.
2) During the dry season, the closed-tide gate condition allowed the development of nitrification, denitrification and the assimilatory NO_3^--N uptake by phytoplankton along the river. These biochemical processes resulted in the prominent decrease in NH_4^+-N concentrations and

increase in NO_3^--N concentrations with time in the lower section of Lianjiang River.

3) Along the river, the difference between nitrification and denitrification rates turned from positive to negative values, and a significant amount of N was removed from the river due to this net effect of nitrification and denitrification.

This study clearly suggests the closed-tide gate condition promotes riverine self-purification. However, more studies are needed to further understand the impacts of seawater intrusion and other biochemical processes such as anammox, to better predict the N flux into estuaries.

Data availability

Data will be made available on request.

Declaration of competing interest

The authors declare that they have no known competing financial interests or personal relationships that could have appeared to influence the work reported in this paper.

Acknowledgments

This work was jointed supported by the Key-Area Research and Development Program of Guangdong Province (Grant Nos.: 2020B1111350001 & 2019B110205003), and the Basal Specific Research of the Central Public-Interest Scientific Institute (Grant No. PM-zx703-202004-141). YH and YX are also grateful to the financial support of the Department of Education of Guangdong Province (No.: 2021ZDZX4016), the Science and Technology Planning Project of Shantou, Guangdong Province, China (No.: STKJ2021112). The authors also thank the anonymous reviewer for constructive feedback.

Appendix A. Supplementary data

Supplementary data to this article can be found online at https://doi.org/10.1016/j.scitotenv.2023.163363.

References

Andersson, M.G.I., Brion, N., Middelburg, J.J., 2006. Comparison of nitrifier activity versus growth in the Scheldt estuary - a turbid, tidal estuary in northern Europe. Aquat. Microb. Ecol. 42, 149–158. https://doi.org/10.3354/ame042149.

Stumm, W., Morgan, J.J., 1996. Aquatic chemistry: chemical equilibria and rates in natural waters. Choice Reviews Online33. https://doi.org/10.5860/choice.33-6312.

Ator, S.W., Garcia, A.M., 2016. Application of SPARROW modeling to understanding contaminant fate and transport from uplands to streams. J. Am. Water Resour. Assoc. 52, 685–704. https://doi.org/10.1111/1752-1688.12419.

Birgand, F., Skaggs, R.W., Chescheir, G.M., Gilliam, J.W., 2007. Nitrogen removal in streams of agricultural catchments - a literature review. Crit. Rev. Environ. Sci. Technol. 37, 381–487. https://doi.org/10.1080/10643380600966426.

Blaen, P.J., Khamis, K., Lloyd, C.E.M., Bradley, C., Hannah, D., Krause, S., 2016. Real-time monitoring of nutrients and dissolved organic matter in rivers: capturing event dynamics, technological opportunities and future directions. Sci. Total Environ. 569–570, 647–660. https://doi.org/10.1016/j.scitotenv.2016.06.116.

Burns, D.A., Pellerin, B.A., Miller, M.P., Capel, P.D., Tesoriero, A.J., Duncan, J.M., 2019. Monitoring the riverine pulse: applying high-frequency nitrate data to advance integrative understanding of biogeochemical and hydrological processes. Wiley Interdiscip. Rev. Water 6, 1–24. https://doi.org/10.1002/wat2.1348.

Butturini, A., Alvarez, M., Bernał, S., Vazquez, E., Sabater, F., 2008. Diversity and temporal sequences of forms of DOC and NO3- discharge responses in an intermittent stream: predictable or random succession? J. Geophys. Res. Biogeosci. 113, G03016. https://doi.org/10.1029/2008JG000721.

Caraco, N.F., Cole, J.J., 1999. Human impact on nitrate export: an analysis using major world rivers. Ambio 28, 167–170. https://doi.org/10.2307/4314870.

Chapra, S.C., di Toro, D.M., 1991. Delta method for estimating primary production, respiration, and reaeration in streams. J. Environ. Eng. 117, 640. https://doi.org/10.1061/(asce)0733-9372(1991)117:5(640).

Chen, F., Jia, G., Chen, J., 2009. Nitrate sources and watershed denitrification inferred from nitrate dual isotopes in the Beijiang River, South China. Biogeochemistry 94, 163–174. https://doi.org/10.1007/s10533-009-9316-x.

Damashek, J., Casciotti, K.L., Francis, C.A., 2016. Variable nitrification rates across environmental gradients in turbid, nutrient-rich estuary waters of San Francisco Bay. Estuar. Coasts 39, 1050–1071. https://doi.org/10.1007/s12237-016-0071-7.

Fazekas, H.M., Wymore, A.S., McDowell, W.H., 2020. Dissolved organic carbon and nitrate concentration-discharge behavior across scales: land use, excursions, and misclassification. Water Resour. Res. 56, 1–14. https://doi.org/10.1029/2019WR027028.

Hall, R.O., Tank, J.L., 2003. Ecosystem metabolism controls nitrogen uptake in streams in grand Teton National Park, Wyoming. Limnol. Oceanogr. 48, 1120–1128. https://doi.org/10.4319/lo.2003.48.3.1120.

Hamrick, J.M., 1992. A three-dimensional environmental fluid dynamics computer code: theoretical and computational aspects. Special Report in Applied Marine Science and Ocean Engineering; No.:317. Virginia Institute of Marine Science, US.

Hill, A.R., Sanmugadas, K., 1985. Denitrification rates in relation to stream sediment characteristics. Water Res. 19, 1579–1586. https://doi.org/10.1016/0043-1354(85)90403-8.

House, W.A., Leach, D.V., Armitage, P.D., 2001. Study of dissolved silicon, and nitrate dynamics in a fresh water stream. Water Res. 35, 2749–2757. https://doi.org/10.1016/S0043-1354(00)00548-0.

Jansson, M., Andersson, R., Berggren, H., Leonardson, L., 1994. Wetlands and lakes as nitrogen traps. Ambio 23, 320–325. https://doi.org/10.1016/0925-8574(95)90014-4.

Jarvie, H.P., Sharpley, A.N., Kresse, T., Hays, P.D., Williams, R.J., King, S.M., Berry, L.G., 2018. Coupling high-frequency stream metabolism and nutrient monitoring to explore biogeochemical controls on downstream nitrate delivery. Environ. Sci. Technol. 52, 13708–13717. https://doi.org/10.1021/acs.est.8b03074.

Jones, A.E., Hodges, B.R., McClelland, J.W., Hardison, A.K., Moffett, K.B., 2017. Residence-time-based classification of surface water systems Allan. Water Resour. Res. 53, 5567–5587. https://doi.org/10.1111/j.1752-1688.1969.tb04897.x.

Koutrakis, E.T., Triantafillidis, S., Sapounidis, A.S., Vezza, P., Kamidis, N., Sylaios, G., Comoglio, C., 2019. Evaluation of ecological flows in highly regulated rivers using the mesohabitat approach: a case study on the Nestos River, N. Greece. Ecohydrology and Hydrobiology 19, 598–609. https://doi.org/10.1016/j.ecohyd.2018.01.002.

Kraus, T.E.C., O'Donnell, K., Downing, B.D., Burau, J.R., Bergamaschi, B.A., 2017. Using paired in situ high frequency nitrate measurements to better understand controls on nitrate concentrations and estimate nitrification rates in a wastewater-Impacted River. Water Resour. Res. 53, 8423–8442. https://doi.org/10.1002/2017WR020670.

Knapp, J.L.A., Li, L., Musolff, A., 2022. Hydrologic connectivity and source heterogeneity control concentration–discharge relationships. Hydrol. Process. 36, 1–16. https://doi.org/10.1002/hyp.14683.

Lehmann, M.F., Reichert, P., Bernasconi, S.M., Barbieri, A., McKenzie, J.A., 2003. Modelling nitrogen and oxygen isotope fractionation during denitrification in a Lacustrine redox-transition zone. Geochim. Cosmochim. Acta 67, 2529–2542. https://doi.org/10.1016/S0016-7037(03)00085-1.

Lembi, C.A., 2001. Limnology, Lake and river ecosystems. J. Phycol. 37, 1146–1147. https://doi.org/10.1046/j.1529-8817.2001.37602.x.

Lin, J., Chen, N., Wang, F., Huang, Z., Zhang, X., Liu, L., 2020. Urbanization increased river nitrogen export to western Taiwan Strait despite increased retention by nitrification and denitrification. Ecol. Indic. 109, 105756. https://doi.org/10.1016/j.ecolind.2019.105756.

Lloyd, C.E.M., Freer, J.E., Johnes, P.J., Collins, A.L., 2016. Using hysteresis analysis of high-resolution water quality monitoring data, including uncertainty, to infer controls on nutrient and sediment transfer in catchments. Sci. Total Environ. 543, 388–401. https://doi.org/10.1016/j.scitotenv.2015.11.028.

Luo, Z., Shao, Q., Liu, H., 2021. Comparative evaluation of river water quality and ecological changes at upstream and downstream sites of dams/sluices in different regulation scenarios. J. Hydrol. 597, 126290. https://doi.org/10.1016/j.jhydrol.2021.126290.

Meyer, C., Stitt, M., 2001. Nitrate reduction and signalling. In: Lea, P., Morot-Gaudy, J. (Eds.), Plant Nitrogen. Springer, Berlin, Heidelberg, pp. 37–59.

Nilsson, C., Reidy, C.A., Dynesius, M., Revenga, C., 2005. Fragmentation and flow regulation of the World's large river systems. Science 308 (5720), 405–408. https://doi.org/10.1126/science.1107887.

Okyereh, S.A., Ofosu, E.A., Kabobah, A.T., 2019. Modelling the impact of bui dam operations on downstream competing water uses. Water-Energy Nexus 2, 1–9. https://doi.org/10.1016/j.wen.2019.03.001.

Risgaard-Petersen, N., Nielsen, L.P., Blackburn, T.H., 1998. Simultaneous measurement of benthic denitrification, with the isotope pairing technique and the N2 flux method in a continuous flow-through system. Water Res. 32, 3371–3377. https://doi.org/10.1016/S0043-1354(98)00121-3.

Rozemeijer, J., van der Velde, Y., de Jonge, H., van Geer, F., Broers, H.P., Bierkens, M., 2010. Application and evaluation of a new passive sampler for measuring average solute concentrations in a catchment scale water quality monitoring study. Environ. Sci. Technol. 44 (4). https://doi.org/10.1021/es903068h.

Sebilo, M., Billen, G., Grably, M., Mariotti, A., 2003. Isotopic composition of nitrate-nitrogen as a marker of riparian and benthic denitrification at the scale of the whole Seine River system. Biogeochemistry 63, 35–51. https://doi.org/10.1023/A:1023362923881.

Sebilo, M., Billen, G., Mayer, B., Billiou, D., Grably, M., Garnier, J., Mariotti, A., 2006. Assessing nitrification and denitrification in the seine river and estuary using chemical and isotopic techniques. Ecosystems 9, 564–577. https://doi.org/10.1007/s10021-006-0151-9.

Triska, F.J., Kennedy, V.C., Avanzino, R.J., Reilly, B.N., 1983. Effect of simulated canopy cover on regulation of nitrate uptake and primary production by natural periphyton assemblages. In: Fontaine, T.D., Bartell, S.M. (Eds.), Dynamics of Lotic Ecosystems. Ann Arbor Science Publishers, Michigan, US, pp. 129–160.

van Breemen, N., Boyer, E.W., Goodale, C.L., Jaworski, N.A., Paustian, K., Seitzinger, S.P., Lajtha, K., Mayer, B., van Dam, D., Howarth, R.W., Nadelhoffer, K.J., Eve, M., Billen, G., 2002. Where did all the nitrogen go? Fate of nitrogen inputs to large watersheds in the northeastern U.S.A. Biogeochemistry, 57–58 https://doi.org/10.1023/A:1015775225913.

van Kessel, J.F., 1977. Removal of nitrate from effluent following discharge on surface water. Water Res. 11, 533–537. https://doi.org/10.1016/0043-1354(77)90041-0.

van Looy, K., Tormos, T., Souchon, Y., 2014. Disentangling dam impacts in river networks. Ecol. Indic. 37, 10–20. https://doi.org/10.1016/j.ecolind.2013.10.006.

Wang, X., Wang, C., Wang, P., Chen, J., Miao, L., Feng, T., Yuan, Q., Liu, S., 2018. How bacterioplankton community can go with cascade damming in the highly regulated Lancang-Mekong River basin. Mol. Ecol. 27, 4444–4458. https://doi.org/10.1111/mec.14870.

Wright, G.V., Wright, R.M., Kemp, P.S., 2015. Impact of tide gates on the migration of adult European eels Anguilla anguilla. Estuar. Coasts 38, 2031–2043. https://doi.org/10.1007/s12237-014-9931-1.

Xia, X., Li, S., Shen, Z., 2008. Effect of nitrification on nitrogen flux across sediment-water Interface. Water Environ. Res. 80, 2175–2182. https://doi.org/10.2175/106143008x296505.

Ye, F., Jia, G., Xie, L., Wei, G., Xu, J., 2016. Isotope constraints on seasonal dynamics of dissolved and particulate N in the Pearl River estuary, South China. J. Geophys. Res. Ocean. 121, 8689–8705. https://doi.org/10.1002/2016JC012066.

Yu, D., Chen, N., Cheng, P., Yu, F., Hong, H., 2020. Hydrodynamic impacts on tidal-scale dissolved inorganic nitrogen cycling and export across the estuarine turbidity maxima to coast. Biogeochemistry 151, 81–98. https://doi.org/10.1007/s10533-020-00712-4.

Zarfl, C., Lumsdon, A.E., Berlekamp, J., Tydecks, L., Tockner, K., 2015. A global boom in hydropower dam construction. Aquat. Sci. 77, 161–170. https://doi.org/10.1007/s00027-014-0377-0.

Zhang, W., Li, H., Kendall, A.D., Hyndman, D.W., Diao, Y., Geng, J., Pang, J., 2019. Nitrogen transport and retention in a headwater catchment with dense distributions of lowland ponds. Sci. Total Environ. 683, 37–48. https://doi.org/10.1016/j.scitotenv.2019.05.171.

Zhao, C., Yang, H., Fan, Z., Zhu, L., Wang, W., Zeng, F., 2020. Impacts of tide gate modulation on ammonia transport in a semi-closed estuary during the dry season-a case study at the Lianjiang river in South China. Water (Switzerland) 12, 1945. https://doi.org/10.3390/w12071945.

Zhao, Q., Wang, Jing, Wang, Jianjian, Wang, J.X.L., 2019. Seasonal dependency of controlling factors on the phytoplankton production in Taihu Lake, China. J. Environ. Sci. (China) 76, 278–288. https://doi.org/10.1016/j.jes.2018.05.010.

Zhao, Y., Xia, Y., Ti, C., Shan, J., Li, B., Xia, L., Yan, X., 2015. Nitrogen removal capacity of the river network in a high nitrogen loading region. Environ. Sci. Technol. 49 (3), 1427–1435. https://doi.org/10.1021/es504316b.

Zheng, L., Cardenas, M.B., Wang, L., 2016. Temperature effects on nitrogen cycling and nitrate removal-production efficiency in bed form-induced hyporheic zones. J. Geophys. Res. Biogeosciences 121, 1086–1103. https://doi.org/10.1002/2015JG003162.